Trajectory Tracking via Independent Solutions to the Geometric and Temporal Tracking Subproblems

Satyajit Ambike[1]
Department of Mechanical Engineering,
The Ohio State University,
Columbus, OH 43210
e-mail: ambike.1@osu.edu

James P. Schmiedeler
e-mail: schmiedeler.4@nd.edu

Michael M. Stanišić
e-mail: stanisic.4@nd.edu

Aerospace and Mechanical Engineering,
University of Notre Dame,
Notre Dame, IN 46556

Trajectory tracking is accomplished by obtaining separate solutions to the geometric path-tracking problem and the temporal tracking problem. A methodology enabling the geometric tracking of a desired planar or spatial path to any order with a nonredundant manipulator is developed. In contrast to previous work, the equations are developed using one of the manipulator's joint variables as the independent parameter in a fixed global frame rather than a configuration-dependent canonical frame. Both these features provide significant practical advantages. Furthermore, a strategy for determining joint velocities and accelerations at singular configurations is provided, which allows the manipulator to approach and/or move out of a singular configuration with finite joint velocities without sacrificing the geometric fidelity of tracking. An example shows a spatial six-revolute robot tracking a trajectory using the developed method in conjunction with resolved-acceleration feedback control. [DOI: 10.1115/1.4003272]

1 Introduction

Spatial trajectory tracking requires that the end-effector (EE) of a manipulator follows a trajectory that is usually prescribed as a function of time. The solution to this problem involves inverting the robot's forward kinematic map, and typically, a local second-order inverse solution (i.e., joint velocities and accelerations) is obtained via inversion of the Jacobian of this map [1]. Often, a variant, called the *manipulator Jacobian* [2], is used in place of the Jacobian of the kinematic map to obtain this solution. This solution, in conjunction with an appropriate feedback control law, such as resolved-acceleration control [3], is utilized to track the desired output-space trajectory in real time. In another approach to trajectory tracking, the joint-space solution for the entire output-space trajectory is computed offline, and the precomputed solution is implemented in conjunction with appropriate feedback control. An elegant way to perform the offline computation is to generate a local high-order approximation of the joint-space solution and then use continuation-like predictor-corrector algorithms to obtain the entire solution [4].

At singular points of the kinematic map, the dimension of the tangent space of the robot is reduced. Therefore, an arbitrary EE velocity is not achievable with finite joint velocities. Irrespective of the commanded speed (a scalar multiple of the path variable time derivative), the EE must stop at a singularity to ensure geometric tracking accuracy. Clearly, this requires explicit control of the path variable. Consequently, any parameterization of the kinematic map that does not allow explicit control of the path variable will fail to impose the above dwell condition. This is reflected in the Jacobian in Ref. [1] becoming ill conditioned in the vicinity of singularities, and the map cannot be inverted at all at a singular configuration via this Jacobian. On the other hand, if the path variable is considered a dependent variable in the parameterization of the kinematic map, its inversion is well-conditioned at and in the vicinity of certain singularities, and the geometric accuracy of tracking is preserved as well.

Several approaches tackle the problem of trajectory tracking in the vicinity of singularities, and Refs. [5,6] provide comprehensive reviews of these methods. However, not all methods explicitly control the path variable along with the trajectory geometry. The Jacobian transpose method [7], the singular value decomposition method [1], and the damped least-squares method [8] are examples. Using the Jacobian transpose instead of the inverse at singular configurations yields joint velocities that minimize the squared norm of the position error. The singular-value-decomposition technique tracks only the component of the task-space velocity that lies in the tangent space of the singular robot. The damped least-squares technique gives an approximate solution that is well-conditioned and defined everywhere in the manipulator's workspace [5,6]. This method modifies the EE path in terms of speed and direction so that the singularity is simply avoided [9]. These techniques aim not to impose a dwell in the path variable, but to obtain bounded joint velocities in the vicinity of a singularity and at the same time, be geometrically as accurate as possible. The geometrical imprecision intrinsic to these methods is a result of not separating the control of the path variable from the control of the trajectory geometry.

The offline computation of the joint-space trajectory [4] treats the path variable as a dependent variable. In fact, the premise of the approach is that the joint-space trajectory corresponding to a given task-space trajectory is a curve in the $(N+1)$-dimensional space of N joint displacements of the N-degree-of-freedom (DOF) mechanism augmented with the path variable used to parameterize the task-space path. This curve is obtained as a function of an auxiliary variable via a predictor-corrector algorithm so that dwells in none of the $N+1$ variables can disrupt the tracking process [4,10]. (This is despite the fact that the examples given in Ref. [4] use joint variables as the independent parameter.) Other parameterizations of the joint-space curve near singularities using fractional power series also exist [11]. The inherent singularity-robustness of the approach in Refs. [4,10] was utilized for singularity navigation in Refs. [9,12], wherein the adjoint of the Jacobian and the null space of an augmented Jacobian, respectively, are used. In Ref. [12], first-order joint motions for nonsingular as well as singular configurations of a six-DOF mechanism are obtained. The nonzero joint velocities obtained force the EE velocity to vanish at the singularity. Therefore, the tracking solution is

[1]Corresponding author.

Contributed by the Mechanisms and Robotics Committee of ASME for publication in the Journal of Mechanisms and Robotics. Manuscript received August 16, 2010; final manuscript received November 24, 2010; published online April 7, 2011. Assoc. Editor: Federico Thomas.

geometrically accurate to the zeroth order, i.e., instantaneously, the EE stays on the desired path, but when it starts to move, the direction of motion does not necessarily coincide with the desired path tangent. The applicability of this first-order approach for real-time trajectory tracking was identified, but not implemented. Higher-order methods that address the geometric tracking accuracy of order greater than zero in singular configurations exist as well [13,14]. In Ref. [13], only wrist-partitioned manipulators are studied, while Ref. [14] analyzes point trajectories for some serial and parallel manipulators.

Another aspect of the approach in Refs. [4,10] is that nontemporal joint-space solutions are obtained by choosing a nontemporal, independent auxiliary variable. Timing is added by specifying the relation between the auxiliary variable and time [4]. In keeping with the offline computation paradigm, Refs. [5,15] assume that the entire time-invariant joint-space solution to a tracking task is available and provide an algorithm to generate temporal joint motions that allow the EE to navigate the given trajectory in near minimal time without geometric deviation at singularities. A key feature of this work, relevant to the present paper, is that it shows that a joint variable can be used to describe the solution curve in the vicinity of singular points [5], and does so to obtain the time-optimal solution near singularities. However, the approach does not allow the speed of the task-space path to be user defined.

The utility of the method in Refs. [4,10] in describing the instantaneous kinematics of the robot is recognized. However, to the best of the authors' knowledge, a strategy for online trajectory tracking through singularities using general six-DOF serial robots has not been developed. The present paper solves the inverse-kinematic problem up to any order for nonsingular configurations, and up to order three explicitly for ordinary singularities[2], and achieves trajectory tracking through singularities without geometric deviation for a general six-DOF serial robot, while performing the entire calculation online. Particularly, joint velocity and acceleration solutions at first-order singular configurations (defined later) are provided. The algorithm is used in conjunction with feedback control to correct for the inaccuracies inherent in the implementation of an approximate local solution. The geometric error in the vicinity of a singularity is an artifact of the local nature of this joint-space solution and not of the singularity in the kinematic map.

This paper argues that it is desirable to choose a joint variable as the independent variable to obtain the instantaneous, time-invariant, inverse-kinematic solution for the real-time trajectory-tracking problem at all points, *not just in the vicinity of singularities*, in contrast to the approach in Ref. [4]. The joint variable used to parameterize the joint-space solution will be called the *leading joint variable*. Practically, it is easier to obtain measurements of the joint variables compared with an arbitrary, nonexistent auxiliary variable or the nontemporal path variable. However, the problem of the leading joint variable encountering a dwell in its trajectory must be tackled. This paper shows how to predict the occurrence of such an event, how to select a nondwelling joint variable to lead the motion and that at least one joint is available to lead the motion for any nonsingular or singular configuration. Another motivation for using the joint-angle variable for solving inverse kinematics comes from the field of human motor control. Based on experimental evidence such as speed-invariant wrist paths for reaching motion [16], it has been proposed that the time-invariant approach outlined herein may describe how the human central nervous system achieves control of arm motion [17]. Other theories, such as the leading joint hypothesis [18], independently propose that the central nervous system may be using the leading joint concept. For a particular reaching motion, the shoulder produces gross torques that are designed to take the wrist in the general vicinity of the target. The elbow controls simply the interaction torque to achieve the specific movement objective. Thus, the shoulder can be viewed as the leading joint. This strategy simplifies the control problem in the dynamic regime. Furthermore, kinesthesia gives humans a sense of joint position, whereas they do not have such a direct means of measuring quantities like arc length. This echoes the motivation for using a single joint angle as the input.

The idea of treating the trajectory-tracking problem as independent geometric and temporal subproblems has another historical precedent. This begins with the curvature theory [19], where general characterization of planar motion is achieved using arbitrary motion parameters. In Ref. [20], two-DOF curvature theory [19] is first generalized to arbitrary DOFs, where the motion of a controlled point on the EE is obtained as a function of two arbitrary motion parameters in a canonical reference frame. The theory is then applied to the problem of generating the joint-space solution to a path-tracking task using a planar, two-DOF mechanism with the joint variables as the independent parameters. Taylor series are used to relate the motion of all joint variables to that of the leading joint variable, rather than to an auxiliary parameter as was the case in Ref. [4]. The coefficients of the Taylor series are called *speed ratios*, and the technique obtains expressions for the speed ratios as functions of the instantaneous invariants (II's) of motion. The II's are geometric parameters that characterize planar motion [19–21]. The theory has been applied to a planar two-revolute (RR) mechanism and a holonomic cart system in Ref. [20], as well as a planar prismatic-revolute (RP) mechanism in Ref. [22]. However, solutions up to only the second order are obtained. Third-order solutions were obtained for the specific case of tracking planar paths with constant curvature in Ref. [23]. Extension of the planar formulation [20] to second-order path tracking using three-DOF spatial systems that include a planar two-DOF subsystem was achieved in Ref. [24]. The regional structure (i.e., manipulators used only for positioning the EE) of the Stanford Arm (a rotating RP mechanism) was used for demonstration.

The curvature-theory approach is also concerned with finding the most parsimonious description of motion. A canonical system is first located, and general expressions for the speed ratios are obtained in this system [20,24]. Even so, these expressions tend to get unwieldy, and the increased complexity is probably one reason why the curvature-theory approach has not been generalized to arbitrary order and to larger spatial systems. Furthermore, the canonical system is a configuration-dependent reference frame. For a trajectory-tracking application, describing the kinematics in a moving canonical frame necessitates an additional transformation between that frame and a global, fixed frame. Therefore, the canonical frame is less suitable for the application. Another observation is that, in these works [20,22,23], the temporal component of the tracking problem is never explicitly solved, although, presumably, the goal is to achieve trajectory tracking and not just path tracking. The method does achieve tangent tracking in singular poses using second-order joint motions and therefore counts as a "higher-order method" for path tracking as per the terminology used in Ref. [5].

The present paper utilizes ideas from the curvature-theory approach and the offline computation approach and modifies them as follows.

1. It abandons the use of an auxiliary parameter as in Ref. [4] and uses a leading joint variable as in Ref. [20] to generate local, inverse-kinematic solutions.
2. It aims to find a local representation of the joint-space curve in N-dimensional joint space, rather than the $(N+1)$-dimensional space used in Ref. [4]. As a consequence, there are fewer Taylor coefficients (the speed ratios) that are needed to describe the solution. In the process of obtaining the pth-order ratios, the pth-order derivatives of the path variables with respect to the leading joint variable

[2]*Ordinary singularities* are configurations of the robot in which the Jacobian drops rank by 1 *and* the path tangent does not lie in the robot's tangent space. The path variable rate is necessarily zero [5,10]. The desired trajectory intersecting the workspace boundary nontangentially is a typical example.

are also obtained. These quantities are needed only for obtaining the geometric solutions of order greater than p. However, they can be used to reduce the computation involved in obtaining the temporal leading joint motion of the same order.
3. It abandons the canonical frame and develops a new set of equations called *coordination equations* in an arbitrary fixed frame.
4. In Ref. [4], the speed ratios are called *kinematic influence coefficients*, and they are obtained indirectly as functions of the coefficients of the Taylor expansions of the variables in terms of the auxiliary parameter. In this paper, the coordination equations yield the speed ratios directly, implying lower computational complexity.
5. With a convenient feedback control law, it achieves online execution of kinematic tracking through singularities with no a-priori knowledge of the inverse-kinematic solution in any form.

The problem being considered is: given a desired, timed trajectory that passes through an ordinary singularity, achieve kinematic tracking of the trajectory by generating local, inverse-kinematic solutions in real time. The approach in this paper solves the inverse-kinematic problem by obtaining independent solutions to the geometric and the temporal problems and using a resolved-acceleration feedback controller to achieve tracking. The geometric, path-tracking problem for a general, three-DOF robot is solved first, followed by the solution to the corresponding temporal problem. Then, a solution to the larger problem of spatial, rigid-body-guidance using six-DOF serial robots is described as a natural extension of the solutions to the three-DOF problems.

The rest of the paper is organized as follows. Section 2 outlines independent solutions to the geometric and temporal tracking problems for a three-DOF, spatial system. The solutions for the singular case are also provided. Section 3 extends the technique to a spatial six-DOF system. Section 4 uses a 6R mechanism to track a specified trajectory. Section 5 discusses drawbacks and future work, and finally, conclusions are given.

2 The Spatial Three-DOF Problem

2.1 Notation. For the three-DOF spatial trajectory-tracking problem, the joint variables are denoted as μ, ν, and λ for convenience and to maintain consistency with previous curvature-theory literature, e.g., Ref. [19]. The standard Denavit–Hartenberg (DH) system [21] is used for the larger, six-DOF case. A trailing subscript(s) indicates the derivative with respect to the subscript(s). For example, $\bar{r}_\lambda := (d\bar{r}/d\lambda)$. A zero after the subscript(s) indicates that the derivative has been evaluated in the zero position. For example, $\bar{r}_{\lambda\mu 0} := (d^2\bar{r}/d\lambda d\mu)|_0$. The dot notation indicates derivatives with respect to time t. For example, $\dot{\lambda} := (d\lambda/dt)|_0$. The symbols n and k always represent the speed ratios with respect to a leading joint variable. A trailing superscript indicates the order of the ratio. For example, $k^{(3)} := (d^3\nu/d\lambda^3)|_0$. The superscript is omitted for the first-order ratios, so $n^{(1)} := n$.

The solution procedure for spatial three-DOF trajectory tracking involves writing the Taylor series approximations for the desired and the generated trajectories and equating the corresponding terms of the two series. This process is also called establishing a contact between the two functions [25]. Two series are written for each trajectory: one using a geometric variable, i.e., joint variable, as the independent parameter, and the second using time as the independent parameter. This way, the geometric and the temporal aspects of tracking are separated. Establishing contact between the geometric Taylor series is equivalent to matching the Frenet–Serret frames [26] of the desired and generated paths. The solution to the geometric problem relates the motion of the mechanism's joints to the motion of the leading joint. The solution to the temporal problem determines the motion properties of the leading joint. Singularities occur in the generated and/or desired trajectory when some derivatives in the corresponding Taylor series vanish. This paper concentrates on singularities in the generated path that coincide with the singular configurations of the robot. The desired path is assumed to be singularity free. In such cases, the geometric tracking problem can still be solved [20]. The only error is in matching the instantaneous speeds of the desired and generated paths.

2.2 Geometric Path-Tracking. The current configuration of the robot is called the zero position, and the values of the joint angles in the zero position are denoted by μ_0, ν_0, and λ_0. The increments in the joint angles are denoted as μ, ν, and λ, and without loss of generality, the instantaneous values of these joint variables in the zero position are taken to be zero. The forward *position* kinematics of the mechanism are given as $\mathbf{r}: R^3 \rightarrow R^3$ such that $\bar{r}_0 = \mathbf{r}(\mu_0, \nu_0, \lambda_0)$, where $\bar{r}_0$ is the current position of a controlled point on the EE–point P. For the trajectory-tracking problem, define $\bar{r}: R \rightarrow R^3$, so that the image of the map $\bar{r}$ represents a spatial curve generated by point P. A typical definition of this mapping yields $\bar{r}(t)$. However, a different parameterization is obtained here by choosing any *nondwelling* joint of the mechanism (henceforth, arbitrarily λ) as the independent parameter to construct $\bar{r} = \bar{r}(\lambda)$. Section 2.6 describes why a leading joint λ is always available. In the zero position, $\bar{r}(0) = \bar{r}_0$. Furthermore, the function $\bar{r}(\lambda)$ is expressed in an arbitrary, fixed reference frame. This is in contrast to the canonical frame used in the curvature-theory-based approaches to the path-tracking problem. In constructing $\bar{r}(\lambda)$, slaving relations between the joints are imposed with the following Taylor series:

$$\mu = n\lambda + \frac{n^{(2)}}{2}\lambda^2 + \frac{n^{(3)}}{6}\lambda^3 + \cdots$$
$$\nu = k\lambda + \frac{k^{(2)}}{2}\lambda^2 + \frac{k^{(3)}}{6}\lambda^3 + \cdots \tag{1}$$

The coefficients of the series are the *speed ratios*, which are defined as

$$n := \left.\frac{d\mu}{d\lambda}\right|_0, \quad n^{(2)} := \left.\frac{d^2\mu}{d\lambda^2}\right|_0, \quad n^{(3)} := \left.\frac{d^3\mu}{d\lambda^3}\right|_0, \cdots$$

$$k := \left.\frac{d\nu}{d\lambda}\right|_0, \quad k^{(2)} := \left.\frac{d^2\nu}{d\lambda^2}\right|_0, \quad k^{(3)} := \left.\frac{d^3\nu}{d\lambda^3}\right|_0, \cdots$$

There are two ratios for every order of coordination. The generated path can now be approximated by a Taylor series

$$\bar{r}(\lambda) = \bar{r}_0 + \bar{r}_{\lambda 0}\lambda + \bar{r}_{\lambda\lambda 0}\frac{\lambda^2}{2} + \bar{r}_{\lambda\lambda\lambda 0}\frac{\lambda^3}{6} + \cdots \tag{2}$$

Note that $\bar{r}_{\lambda 0} = \bar{r}_{\lambda 0}(n,k)$, $\bar{r}_{\lambda\lambda 0} = \bar{r}_{\lambda\lambda 0}(n,k,n^{(2)},k^{(2)})$, and so on.

The *desired path* is a spatial curve $\bar{R}$ specified in terms of an arbitrary variable q. The function $q(t)$ is also specified. The Taylor series for $\bar{R}$ in terms of λ is given by

$$\bar{R}(s(\lambda)) = \bar{R}_0 + (s_{\lambda 0}\bar{R}_{s0})\lambda + (s_{\lambda\lambda 0}\bar{R}_{s0} + s_{\lambda 0}^2\bar{R}_{ss0})\frac{\lambda^2}{2} + [s_{\lambda\lambda\lambda 0}\bar{R}_{s0} + 3s_{\lambda 0}s_{\lambda\lambda 0}\bar{R}_{ss0} + s_{\lambda 0}^3\bar{R}_{sss0}]\frac{\lambda^3}{6} + \cdots$$

where s is the arc length of the desired path. Using standard relations in differential geometry, this can be rewritten as

$$\bar{R}(s(\lambda)) = \bar{R}_0 + [s_{\lambda 0}\hat{T}]\lambda + [s_{\lambda\lambda 0}\hat{T} + s_{\lambda 0}^2\kappa\hat{N}]\frac{\lambda^2}{2} + [(s_{\lambda\lambda\lambda 0} - \kappa^2 s_{\lambda 0}^3)\hat{T} + (3s_{\lambda 0}s_{\lambda\lambda 0}\kappa + \kappa_{s0}s_{\lambda 0}^3)\hat{N} + \kappa\tau s_{\lambda 0}^3\hat{B}]\frac{\lambda^3}{6} + \cdots \quad (3)$$

Equation (3) uses a local Frenet–Serret frame to describe the instantaneous geometric properties of the desired path [26]. The triad $\hat{T}-\hat{N}-\hat{B}$ is the natural trihedron of the curve formed by the tangent, the normal, and the binormal, respectively. The quantities κ and τ are the curvature and the torsion, respectively, and $\kappa_{s0} = (d\kappa/ds)|_0$. These geometric properties can be obtained from the parametric equation $\bar{R}(q)$ (or $\bar{R}(t)$) using standard relations [26]. For example

$$\hat{T} = \frac{\bar{R}_{q0}}{|\bar{R}_{q0}|} \quad (4)$$

$$\bar{N} = \bar{R}_{qq0} - (\bar{R}_{qq0}\cdot\hat{T})\hat{T}, \quad \hat{N} = \frac{\bar{N}}{|\bar{N}|} \quad (5)$$

$$\hat{B} = \hat{T}\times\hat{N} \quad (6)$$

Expressions for the curvature and torsion are also readily available, and higher-order properties such as κ_{so} are obtained by differentiating these equations. The derivatives of the arc length s with respect to λ also appear in Eq. (3). These are unknown and are the terms of the Taylor series expansion of the function $s(\lambda)$.

The pth-order geometric tracking problem is solved by establishing pth-order contact between the curves $\bar{r}(\lambda)$ and $\bar{R}(\lambda)$ by equating the first $p-1$ derivatives in Eqs. (2) and (3) [25]. Establishing contact (i.e., achieving coordination) proceeds in stages from the zeroth to the third and potentially higher orders. At each stage, it is assumed that all lower orders of coordination (or contact) have been achieved. In equating the derivatives, two things are implied: first, the geometric entities of the two paths, such as the tangent, normal, etc., are forced to be identical; and second, the arc lengths of the two paths are forced to be equal. Therefore, pth-order contact is simultaneously established between the Taylor series for the arc lengths of the two paths, i.e., the function $s(\lambda)$ is being constructed. For each order of coordination except the zeroth order, a 3D vector equation involving two unknown speed ratios and the unknown derivative of the path variable, called *the coordination equation*, is obtained. The solution requires a linear inversion as shown below, in which the general form of the pth-order coordination equation is derived first, followed by the specific forms of this equation for the zeroth and first three orders.

2.3 *p*th-Order Coordination. In Appendix A, it is shown that the pth-derivative of $\bar{r}$ is linear in the pth-order speed ratios. Therefore, for $p=1$, let

$$\bar{r}_\lambda = J_1\frac{d\mu}{d\lambda} + J_2\frac{d\nu}{d\lambda} + J_3 \quad (7)$$

$$\Rightarrow \bar{r}_{\lambda 0} = [J_{10} \quad J_{20} \quad J_{30}]\bar{n}_1 + J_{30} = \mathbf{J}\bar{n}_1 + \bar{\Phi}_0 \quad (8)$$

where the matrix $\mathbf{J}$ is the Jacobian of the function $\mathbf{r}(\mu,\nu,\lambda)$, J_i are the columns of the Jacobian, J_{i0} are the Jacobian columns evaluated at the zero position, $\bar{\Phi}_0 = J_{30}$, and $\bar{n}_1 = [n \;\; k \;\; 0]^T$. Note that this Jacobian is the Jacobian of the kinematic mapping and not the manipulator Jacobian that also appears in robotics literature [2]. Differentiating Eq. (7) and evaluating the result in the zero position

$$\bar{r}_{\lambda\lambda 0} = \{[J_{1\lambda 0} \quad J_{2\lambda 0} \quad J_{3\lambda 0}]\bar{n}_1 + J_{3\lambda 0}\} + \mathbf{J}\begin{bmatrix} n^{(2)} \\ k^{(2)} \\ 0 \end{bmatrix} = \bar{\Phi}_1 + \mathbf{J}\bar{n}_2$$

where $\bar{\Phi}_1$ is a known quantity since $J_{1\lambda 0}$, $J_{2\lambda 0}$, and $J_{3\lambda 0}$ are functions of the mechanism's pose and the first-order speed ratios, and $\bar{n}_2 = [n^{(2)} \;\; k^{(2)} \;\; 0]^T$. With repeated differentiation

$$\bar{r}_{\lambda p0} = \bar{\Phi}_{p-1} + \mathbf{J}\bar{n}_p \quad (9)$$

where $\bar{r}_{\lambda p0} := \bar{r}_{(\lambda\lambda\lambda\ldots \text{p times})0}$. As before, $\bar{\Phi}_{p-1}$ is a known quantity, and $\bar{n}_p = [n^{(p)} \;\; k^{(p)} \;\; 0]^T$.

The pth-order term of the series in Eq. (3) is expressed as

$$\left.\frac{d^p\bar{R}}{d\lambda^p}\right|_0 = u_p\hat{T} + v_p\hat{N} + w_p\hat{B} \quad (10)$$

where u_p, v_p, and w_p are scalar functions of the derivatives of the arc length and the scalar-valued desired path properties like κ, τ, etc. The following structure is observed in these scalar coefficients:

$$u_1 = s_{\lambda 0}, \quad v_1 = 0 \quad w_1 = 0$$

$$u_2 = s_{\lambda\lambda 0}, \quad v_2 = \kappa u_1^2, \quad w_2 = 0 \quad (11)$$

$$u_3 = s_{\lambda\lambda\lambda 0} - \kappa^2 u_1^3, \quad v_3 = 3u_1u_2\kappa + \kappa_{s0}u_1^3, \quad w_3 = \kappa\tau u_1^3$$

The pth-order derivative of the path variable s with respect to the leading joint variable is an unknown quantity. Note that only the coefficient u_p contains this derivative, and therefore, u_p is the only unknown quantity on the right-hand-side (RHS) of Eq. (10).

To establish pth-order contact, the RHS of Eqs. (9) and (10) are equated

$$\bar{\Phi}_{p-1} + \mathbf{J}\bar{n}_p = u_p\hat{T} + v_p\hat{N} + w_p\hat{B} \quad (12)$$

Rearranging Eq. (12) gives the pth-order coordination equation in the general form

$$\mathbf{J}^*\bar{n}_p^* = v_p\hat{N} + w_p\hat{B} - \bar{\Phi}_{p-1} =: \bar{\Psi}_{p-1} \quad (13)$$

where $\mathbf{J}^* := [J_{10} \;\; J_{20} \;\; -\hat{T}]$ and $\bar{n}_p^* := [n^{(p)} \;\; k^{(p)} \;\; u_p]^T$. The matrix $\mathbf{J}^*$ is composed by replacing the column of $\mathbf{J}$ corresponding to the partial derivative of $\mathbf{r}$ with respect to the leading joint variable with $-\hat{T}$. As long as $\mathbf{J}^*$ is full rank, Eq. (13) can be solved for $\bar{n}_p^*$. Note that as long as $\mathbf{J}$ is full rank, it is always possible to obtain a full-rank matrix $\mathbf{J}^*$ by replacing one of the columns of $\mathbf{J}$ by $-\hat{T}$. The trailing subscript $p-1$ for $\bar{\Psi}$ indicates that the quantity depends on up to the $(p-1)$th-order quantities.

The coefficients $u_i, i<p$ are required to solve Eq. (13) since v_p and w_p are functions of u_i. Solving Eq. (13) yields u_p, which is critical only if a joint-space solution of order greater than p is desired. However, it can also be used for computing the pth-order temporal motion of the leading joint, as shown in Sec. 2.4.

Finally, the solution to the coordination equation of any order requires the inversion of the modified Jacobian matrix $\mathbf{J}^*$. This is a consequence of the fact that the pth-order derivative of $\bar{r}$ is always linear in the pth-order speed ratios, and the coordination equation is linear in the coefficient u_p. Therefore, closed-form solutions for the speed ratios of arbitrary order can be obtained for nonsingular configurations.

2.3.1 Zeroth-Order Coordination. This involves achieving the appropriate pose of the mechanism by solving the inverse position kinematics problem. In the foregoing, it is assumed that the EE is on the desired path in the zero position. This is a reasonable assumption to make since the problem of path tracking mainly involves consideration of derivatives of the position, rather than the

position itself. Therefore, rather than explicitly solve the inverse position kinematics problem, it is considered solved by virtue of the current pose of the mechanism.

2.3.2 First-Order Coordination. Substituting $p=1$ in Eq. (13) yields the first-order coordination equation

$$\mathbf{J}^* \bar{n}_1^* = \bar{\Psi}_0 \tag{14}$$

where $\bar{\Psi}_0 = -\bar{\Phi}_0 = -J_{30}$. Equation (14) is solved for the first-order ratios and u_1. Note that the first-order coordination equation also implies $\bar{r}_{\lambda 0} = s_{\lambda 0}\hat{T}$, i.e., the tangents of the desired and the generated paths are forced to be parallel.

2.3.3 Second-Order Coordination. Substituting $p=2$ in Eq. (13) yields the second-order coordination equation

$$\mathbf{J}^* \bar{n}_2^* = \bar{\Psi}_1 \tag{15}$$

From Eqs. (11) and (13), $\bar{\Psi}_1 = \kappa u_1^2 \hat{N} - \bar{\Phi}_1$. Note that the value of u_1 obtained from the first-order coordination equation is required in the second-order equation. Equation (15) is solved for the two second-order speed ratios and u_2.

2.3.4 Third-Order Coordination. Substituting $p=3$ into Eq. (13) yields the third-order coordination equation

$$\mathbf{J}^* \bar{n}_3^* = \bar{\Psi}_2 \tag{16}$$

From Eqs. (11) and (13)

$$\bar{\Psi}_2 = (3u_1 u_2 \kappa + \kappa_{s0} u_1^3)\hat{N} + \kappa\tau u_1^3 \hat{B} - \bar{\Phi}_2$$

As before, u_1 and u_2 are required to solve Eq. (16) for the two third-order speed ratios and u_3.

In Ref. [27], a spatial, 3R mechanism is used to geometrically track a spatial path up to the third order as an example of the implementation of the theoretical development in this section. The 3R mechanism used there resembles the regional structure of the six-DOF manipulator used for the example in Sec. 4 of this paper.

2.4 Temporal Joint-Motion Properties. To complete the solution to the trajectory-tracking problem, the temporal joint-motion properties must be determined. In Ref. [10], the possibility of completing the trajectory-tracking problem by obtaining the joint rates is mentioned, and Ref. [5] solves the problem of obtaining a time-optimal path timing assuming that the joint-space solution is available. In the ongoing, the speed ratios define relations between the temporal joint motions. Therefore, the temporal motion of the leading joint is now obtained, followed by the temporal joint motion of the other "following" joints via the speed ratios.

Similar to the geometric problem, the approach here is to establish pth-order contact between the *time-dependent* Taylor series of the desired and generated paths. Therefore, the functions $\bar{r}(\lambda(t))$ and $\bar{R}(t)$ are expressed as

$$\bar{r}(\lambda(t)) = \bar{r}_0 + (\dot{\lambda}\bar{r}_{\lambda 0})t + (\dot{\lambda}^2 \bar{r}_{\lambda\lambda 0} + \ddot{\lambda}\bar{r}_{\lambda 0})\frac{t^2}{2} + (\dot{\lambda}^3 \bar{r}_{\lambda\lambda\lambda 0} + 3\dot{\lambda}\ddot{\lambda}\bar{r}_{\lambda\lambda 0} + \dddot{\lambda}\bar{r}_{\lambda 0})\frac{t^3}{6} + \cdots \tag{17}$$

$$\bar{R}(t) = \bar{R}_0 + \dot{\bar{R}}t + \ddot{\bar{R}}\frac{t^2}{2} + \dddot{\bar{R}}\frac{t^3}{6} + \cdots \tag{18}$$

Note that the function $q(t)$ is specified. Therefore, the time derivatives of $\bar{R}(q(t))$ can be obtained via the chain rule. The vector $\bar{r}_{p\lambda 0}$ and the coefficient u_p are already available from the solution of the pth-order coordination equation. Using the definition of the arc length of a curve, it can be shown that

$$\bar{r}_{\lambda 0} \cdot \bar{r}_{\lambda 0} = u_1^2, \quad \bar{r}_{\lambda\lambda 0} \cdot \bar{r}_{\lambda 0} = u_1 u_2, \quad \bar{r}_{\lambda\lambda\lambda 0} \cdot \bar{r}_{\lambda 0} = u_1 u_3 \tag{19}$$

Equating the corresponding derivatives of the two series and substituting Eq. (19) into the result yields

$$\dot{\lambda} = \frac{\dot{\bar{R}} \cdot \bar{r}_{\lambda 0}}{\bar{r}_{\lambda 0} \cdot \bar{r}_{\lambda 0}} = \frac{\dot{\bar{R}} \cdot \bar{r}_{\lambda 0}}{u_1^2} \tag{20}$$

$$\ddot{\lambda} = \frac{(\ddot{\bar{R}} - \dot{\lambda}^2 \bar{r}_{\lambda\lambda 0}) \cdot \bar{r}_{\lambda 0}}{\bar{r}_{\lambda 0} \cdot \bar{r}_{\lambda 0}} = \frac{\ddot{\bar{R}} \cdot \bar{r}_{\lambda 0} - \dot{\lambda}^2 u_1 u_2}{u_1^2} \tag{21}$$

$$\dddot{\lambda} = \frac{(\dddot{\bar{R}} - 3\dot{\lambda}\ddot{\lambda}\bar{r}_{\lambda\lambda 0} - \dot{\lambda}^3 \bar{r}_{\lambda\lambda\lambda 0}) \cdot \bar{r}_{\lambda 0}}{\bar{r}_{\lambda 0} \cdot \bar{r}_{\lambda 0}} = \frac{\dddot{\bar{R}} \cdot \bar{r}_{\lambda 0} - 3\dot{\lambda}\ddot{\lambda} u_1 u_2 - \dot{\lambda}^3 u_1 u_3}{u_1^2} \tag{22}$$

and so on for higher-order joint properties. Clearly, the Taylor series for the function $\lambda(t)$ is being constructed. The motion of the following joints can be obtained by differentiating the series in Eq. (1) as

$$\dot{\mu} = n\dot{\lambda}, \quad \dot{\nu} = k\dot{\lambda} \tag{23}$$

$$\ddot{\mu} = n\ddot{\lambda} + n^{(2)}\dot{\lambda}^2, \quad \ddot{\nu} = k\ddot{\lambda} + k^{(2)}\dot{\lambda}^2 \tag{24}$$

$$\dddot{\mu} = n\dddot{\lambda} + 3n^{(2)}\dot{\lambda}\ddot{\lambda} + n^{(3)}\dot{\lambda}^3, \quad \dddot{\nu} = k\dddot{\lambda} + 3k^{(2)}\dot{\lambda}\ddot{\lambda} + k^{(3)}\dot{\lambda}^3 \tag{25}$$

and so on for higher-order derivatives.

2.5 Singularities. A *first-order singularity* is defined as a pose of the mechanism in which the Jacobian rank ($\mathbf{J}$ of the function $\mathbf{r}(\mu, \nu, \lambda)$ introduced in Eq. (8)) drops by 1. The dimension of the tangent space of the manipulator is less than the dimension of the output space of the robot. Therefore, it is impossible for the robot to move along a path tangent that does not lie in its (reduced) tangent space with first-order joint control. The condition $\hat{T} \notin col[\mathbf{J}]$ defines an *ordinary* singularity[3] [5]. The first-order motion of the EE *must* vanish to maintain the fidelity of geometric tracking, i.e.,

$$u_1 = sg_{\lambda 0} = 0, \quad \Rightarrow \bar{r}_{\lambda 0} = \bar{0}$$

where sg is the arc length of the generated path. It is now necessary to draw a distinction between the arc lengths of the desired path and the generated paths. This distinction was unnecessary for the nonsingular case, as the condition $sg := s$ is implied in establishing the contact between the Taylor series for the desired and generated paths. However, in the singular case, the speed of the generated path must vanish ($\dot{sg} = 0$), irrespective of the speed of the desired path. Therefore, the condition $sg := s$ is violated. It is recognized that at singular configurations, there must be a compromise between the speed and the accuracy of tracking [5,8]. The vanishing speed and accurate tangent tracking (demonstrated below) represent one extreme of this compromise. The vanishing speed modifies Eq. (11) as follows:

$$\begin{aligned} u_1 &= sg_{\lambda 0} = 0, \quad v_1 = 0, \quad w_1 = 0 \\ u_2 &= sg_{\lambda\lambda 0}, \quad v_2 = 0, \quad w_2 = 0 \\ u_3 &= sg_{\lambda\lambda\lambda 0}, \quad v_3 = 0, \quad w_3 = 0 \end{aligned} \tag{26}$$

[3] At a *nonordinary* singularity or *bifurcation*, $\hat{T} \in col[\mathbf{J}]$ [28]. The term "bifurcation" represents the intersection of multiple solution branches in the joint space. These are discussed in Appendix C.

Note that u_2 and u_3 are not zero.

Since, for a first-order ordinary singularity, rank$[\mathbf{J}]=2$ and $\hat{T} \notin col[\mathbf{J}]$, it is possible to construct $\mathbf{J}^*$ such that rank$[\mathbf{J}^*]=3$. Therefore, Eqs. (14)–(16) are applicable for ordinary singularities. Further, since rank$[\mathbf{J}^*]=3$, Eq. (14) can be expressed as

$$\begin{bmatrix} J_1 & J_2 & -\hat{T} \end{bmatrix} \begin{bmatrix} n \\ k \\ u_1 \end{bmatrix} = aJ_1 + bJ_2 \tag{27}$$

where a and b are some scalars. The condition $u_1=0$ is imposed by Eq. (14), as can be seen from the solution to its variant given by Eq. (27). This is an advantage of the present method. *There is no change in the strategy for obtaining speed ratios at or in the vicinity of an ordinary singularity.* Furthermore, Eq. (27) can be expressed as

$$\mathbf{J} \begin{bmatrix} n \\ k \\ 1 \end{bmatrix} = \bar{0} \tag{28}$$

Equation (28) has a unique, nontrivial solution that belongs to the null space of the singular Jacobian. Therefore, the solution obtained by Eq. (14) is similar to the null-space solution in Ref. [12].

In a singular configuration, since $\bar{r}_{\lambda 0}=\bar{0}$, Eq. (2) becomes

$$\bar{r}(\lambda) = \bar{r}_0 + \bar{r}_{\lambda\lambda 0}\frac{\lambda^2}{2} + \bar{r}_{\lambda\lambda\lambda 0}\frac{\lambda^3}{6} + \cdots \tag{29}$$

Furthermore, since the speed of the generated path vanishes in the singular configuration, the speed of the desired path is also assumed to be zero, $s_{\lambda 0}=0$, and Eq. (3) becomes

$$\bar{R}(s(\lambda)) = \bar{R}_0 + (s_{\lambda\lambda 0}\hat{T})\frac{\lambda^2}{2} + (s_{\lambda\lambda\lambda 0}\hat{T})\frac{\lambda^3}{6} + \cdots \tag{30}$$

If the desired speed in the singular configuration is nonzero, the present formulation will result in error in tracking the arc length. However, second- and third-order coordination, as imposed by Eqs. (15) and (16), force the vectors $\bar{r}_{\lambda\lambda 0}$ and $\bar{r}_{\lambda\lambda\lambda 0}$, respectively, to be parallel to $\hat{T}$. Comparing the second and third terms in Eqs. (29) and (30) makes this clear. Thus, the geometry of the desired and generated paths is matched, but, in general, the evolutions of the arc lengths of the desired and generated paths are not instantaneously identical.

It is worthwhile to point out that although $s_{\lambda 0}=0$, the definitions given in Eqs. (4)–(6) are valid as long as the desired path does not have a singularity. As expected, it is still possible to track the desired path tangent. However, notice that third-order coordination manages only tangent tracking in the singular case, compared with matching the third-order path properties for a nonsingular pose. Therefore, the control of the path geometry has degraded in the singular pose.

The time-based joint motions are obtained next. The evolution of sg is

$$sg(t) = sg_{\lambda\lambda 0}\dot{\lambda}^2\frac{t^2}{2!} + (sg_{\lambda\lambda\lambda 0}\dot{\lambda}^3 + 3sg_{\lambda\lambda 0}\dot{\lambda}\ddot{\lambda})\frac{t^3}{3!} + \cdots$$

For the nonsingular case, the quantity $sg_{\lambda\lambda 0}$ is obtained by differentiating the expression for the arc length of the generated curve with respect to λ, and it is the component of $\bar{r}_{\lambda\lambda 0}$ along the desired tangent $\hat{T}$. Since, for the singular case, Eq. (15) forces $\bar{r}_{\lambda\lambda 0}$ to be parallel to $\hat{T}$, define

$$sg_{\lambda\lambda 0} := \sqrt{\bar{r}_{\lambda\lambda 0} \cdot \bar{r}_{\lambda\lambda 0}} \tag{31}$$

The quantity $sg_{\lambda\lambda\lambda 0}$ is obtained by differentiating Eq. (31) with respect to λ and evaluating the result in the zero position. From Eq. (26), the quantities $sg_{\lambda\lambda 0}$ and $sg_{\lambda\lambda\lambda 0}$ are u_2 and u_3, respectively, and they are obtained from the solution to the second- and third-order coordination equations. One approach to find the leading joint motion is to ignore the mismatch in the trajectory speeds and match the tangential acceleration and tangential jerk magnitudes of the desired and generated paths by equating the second- and third-order terms of the time-based Taylor series given by Eqs. (17) and (18). This yields

$$\dot{\lambda} = \pm\sqrt{\frac{\ddot{\bar{R}} \cdot \bar{r}_{\lambda\lambda 0}}{\bar{r}_{\lambda\lambda 0} \cdot \bar{r}_{\lambda\lambda 0}}} = \pm\sqrt{\frac{\ddot{s}}{u_2}} \tag{32}$$

$$\ddot{\lambda} = \frac{(\dddot{\bar{R}} - \dot{\lambda}^3\bar{r}_{\lambda\lambda\lambda 0}) \cdot \bar{r}_{\lambda\lambda 0}}{3\dot{\lambda}\bar{r}_{\lambda\lambda 0} \cdot \bar{r}_{\lambda\lambda 0}} = \frac{\dddot{s} - \dot{\lambda}^3 u_3}{3\dot{\lambda}u_2} \tag{33}$$

Equations (32) and (33) give two valid solutions. If the commanded speed at the singularity is zero, these solutions are exact. Otherwise, the error in tracking the arc length is of the order $(\dot{s} * \Delta t)$, where Δt is the elapsed time. Another approach to obtain the leading joint motions is to solve for the joint velocity using Eq. (32) and then equate the arc lengths s and sg after time Δt. The time interval can be based on the feedback frequency of the tracking system. Therefore

$$s(\Delta t) = sg(\Delta t) = u_2\dot{\lambda}^2\frac{(\Delta t)^2}{2} + (u_3\dot{\lambda}^3 + 3u_2\dot{\lambda}\ddot{\lambda})\frac{(\Delta t)^3}{6} \tag{34}$$

Equation (34) is solved for $\ddot{\lambda}$. Equation (34) could also be used to choose between the two solutions generated by Eqs. (32) and (33). Equation (23) is used to determine the velocities of the other joints, and they ensure that the joint velocity vector belongs to the null space of the singular Jacobian. Next, Eq. (24) are used to compute the joint accelerations.

It is important to mention that specifying the joint velocities alone will not achieve tangent tracking. It is Eq. (15), which requires the specification of $\bar{r}_{\lambda\lambda 0}$, that achieves tangent tracking. This imposes a constraint on the joint accelerations via the second-order speed ratios (Eq. (24)). This is consistent with previous work [20], wherein higher-order joint motions are used to obtain the desired EE motion geometry of a lower order. However, note that although the second-order analysis constrains the joint accelerations, it does not provide a means of computing the leading joint acceleration itself. Here, the third-order analysis is used to compute the leading joint acceleration (via u_3), and it simultaneously constrains the joint jerks (via the third-order speed ratios) without providing the means to compute the leading joint jerk. Therefore, with the suggested strategy, *third-order coordination is necessary to obtain the geometric and temporal solutions to the first-order trajectory-tracking problem at ordinary singularities.* From a practical standpoint, third-order coordination imposes a higher computational load on the tracking system.

In conclusion, for a first-order singular pose of the mechanism, the zeroth- and first-order joint coordination together match the position properties of the desired trajectory, and the second- and third-order coordination together match the first-order properties of the desired trajectory. A pattern seems to be emerging, wherein two terms of the Taylor series of the generated trajectory account for each term in the Taylor series of the desired trajectory. However, this requires further investigation.

2.6 Choosing a Nondwelling Leading Joint. An alternate expression for the pth-order speed ratio is given by Eq. (B2) in Appendix B, where the ratio is obtained as a function of the previous $p-1$ ratios and the time derivatives of the joint variables up to the pth-order. As the current leading joint approaches a dwell in its trajectory, $\dot{\lambda} \to 0$, and from Eq. (B2), the corresponding speed ratios approach infinity. This phenomenon can be conveniently used to detect the occurrence of a dwell in λ. The speed ratios corresponding to different leading joints are related with simple algebraic expressions

$$\left.\frac{d\lambda}{d\mu}\right|_0 = \frac{1}{n}, \qquad \left.\frac{d\nu}{d\mu}\right|_0 = \frac{k}{n}$$

$$\left.\frac{d^2\lambda}{d\mu^2}\right|_0 = -\frac{n^{(2)}}{n^3}, \qquad \left.\frac{d^2\nu}{d\mu^2}\right|_0 = \frac{nk^{(2)} - kn^{(2)}}{n^3}$$

and so on for higher orders, as well as for ratios with ν as the leading joint variable. Note that if $n \to \infty$, the ratios with either μ or ν as the leading joint variable will necessarily be small. With checks on the absolute magnitudes of the speed ratios, a nondwelling leading joint can be chosen.

At least one joint of the mechanism must move for the EE to possess some velocity. Therefore, there is at least one joint capable of serving as the leading joint. A possible difficulty is in choosing the leading joint when the EE speed vanishes. This occurs at singular configurations where the EE speed is forced to vanish. However, since the Jacobian is singular, it is possible to obtain a nonzero joint velocity vector belonging to the null space of the Jacobian, thus making a leading joint available. Another scenario is when the robot begins to move from a nonsingular configuration, but the EE velocity remains zero. The geometric problem is well defined, assuming that the desired path is singularity free, and the coordination equations can be solved. Equations (20) and (23) ensure that the generated EE velocity will vanish.

A dwell in the leading joint is governed by the current configuration of the mechanism and the direction of the desired tangent. Therefore, a dwell can occur anywhere in the workspace of the robot. The proximity of the leading joint to a dwell is reflected in the modified Jacobian $\mathbf{J}^*$ becoming ill conditioned and the corresponding speed ratios becoming large in magnitude. Several manipulability measures, such as the smallest singular value of the Jacobian [29] and the condition number of the Jacobian [30], exist that measure the distance of a robot's configuration from a singularity. The absolute values of the speed ratios perform the function of such measures as applied to $\mathbf{J}^*$ in order to identify proximity to a dwell in the current leading joint.

The proximity of the robot's configuration to a singularity *alone* does not influence the occurrence of a dwell in the leading joint. Therefore, the speed ratios associated with the appropriate choice of a leading joint are well behaved in the neighborhood of an ordinary singularity. This provides a strategy to obtain bounded joint rates in the vicinity of an ordinary singularity. It is only *at* the singular configuration where a change in the computation strategy is required. The equations for obtaining the velocity and acceleration of the leading joint change, as shown in Sec. 2.5. One expects that the only realistic scenario in which these alternate equations would be applicable is when the robot begins its motion from a singular configuration. Finally, it is possible that all possible variants of $\mathbf{J}^*$ are ill conditioned. This indicates the proximity of $\hat{T}$ to the reduced tangent space of the robot, i.e., this condition is close to a *nonordinary singularity* which is discussed in Appendix C.

3 Six-DOF Manipulators

3.1 Notation. For the spatial rigid-body guidance problem, the DH parameters [2] are used to describe the kinematics of the robot. The joint-space vector is $\bar{\theta}$ containing the joint variables θ_i, $i=1\ldots6$. Assuming θ_1 to be the leading joint variable, the jth-order speed ratio relating the motion of joint i to that of the leading joint when evaluated in the zero position is denoted by $n_i^{(j)}$. Therefore, $n_3^{(3)} := (d^3\theta_3/d\theta_1^3)|_0$. For $j=1$, the superscript is omitted, so $n_2^{(1)} := n_2 = (d\theta_2/d\theta_1)|_0$. There will be five speed ratios for each order and five joint-coordinating Taylor series similar to those in Eq. (1).

A rigid-body guidance problem is specified by defining the time evolution of a homogeneous transformation matrix $\mathbf{H}(t)$, where $\mathbf{H} \in SE(3)$ [2]. The task specification in this form is not suitable for employing the methods of this paper precisely because it does not separate the geometric and the temporal tracking problems. However, there are two equivalent representations that achieve this separation, and both representations can be obtained from $\mathbf{H}(t)$. In the first, the translational motion of one convenient *control point* on the EE is obtained by constructing the function $\bar{R}(t)$ using standard velocity, acceleration, and jerk relations. Then, the local geometric properties of the control-point path are obtained from relations of the form given in Eqs. (4)–(6). Next, the angular velocity and acceleration of the EE are related to the Darboux vector and its derivative [26]. However, computing these quantities requires higher-order derivatives (κ_{s0} and τ_{s0}) of the control-point path, as shown in Ref. [31]. Therefore, the ensuing development in this paper adopts the second representation which describes the EE translation and rotation by specifying the translation of three noncollinear control points on the EE. The use of three points on the EE to characterize its motion was introduced in Ref. [32] to develop dimensionally homogeneous dexterity measures. It is shown in Ref. [32] that no representational singularities are introduced by this method provided the points are noncollinear. The desired translations of the three control points are obtained exactly as described in the first representation above, and the methods of the previous sections are applied with minimal modification. By writing coordination equations for three points, a sufficient number of equations are generated to obtain the five speed ratios of each order and the unknown path variable derivatives for the paths of the three points.

Let $\bar{P}_i$, $i=1,2,3$ denote the three control points on the EE. Then, the position kinematics of the system are described as

$$\bar{r}_i(\bar{\theta}) = \bar{P}_i, \quad i = 1,2,3 \tag{35}$$

Equation (35) consists of nine component equations that are subject to three rigid-body constraints (RBCs) stating that the distances between the three control points are constant. The desired path is specified next by specifying the paths for the control points in terms of parameters q_i: $\bar{P}_i = \bar{P}_i(q_i)$. Equation (35) is modified to describe the tracking problem

$$\bar{r}_i(\bar{\theta}) - \bar{P}_i(q_i) = 0, \quad i = 1,2,3 \tag{36}$$

A valid task specification must also respect the RBC. Therefore, given any one of the path variables, $q_1 = q_1^*$, say, the other two can be computed using the RBC. Consequently, there is only one independent motion variable for the desired path, and Eq. (36) represents a system of six equations in the seven unknown motion parameters $\bar{\theta}$ and q_1. The locus of solutions to Eq. (36) represents a set of curves in the seven-dimensional space of the motion parameters. According to the implicit function theorem, the solution curve can be locally described in terms of one of the variable parameters in the vicinity of a given configuration $(\bar{\theta}^*, q_1^*)$ that satisfies Eq. (36) if the Jacobian of the equation system in Eq. (36) has rank six. The Jacobian is constructed as follows:

$$\mathbf{J} = [\mathbf{J}' \quad \mathbf{P}'] = \begin{bmatrix} \mathbf{J}_1 & \dfrac{d\bar{P}_1}{dq_1} \\ \mathbf{J}_2 & \dfrac{d\bar{P}_2}{dq_2}\dfrac{dq_2}{dq_1} \\ \mathbf{J}_3 & \dfrac{d\bar{P}_3}{dq_3}\dfrac{dq_3}{dq_1} \end{bmatrix} \tag{37}$$

where $\mathbf{J}_i$ is a Jacobian matrix of order 3×6 similar to that occurring in Sec. 2.3. The order of $\mathbf{J}$ is 9×7. The matrix $\mathbf{J}'$ can be evaluated at the given configuration $\bar{\theta}^*$. The coefficients (dq_i/dq_1) at q_i^* are obtained by differentiating the RBC with respect to q_1 as follows. For $i=2,3$

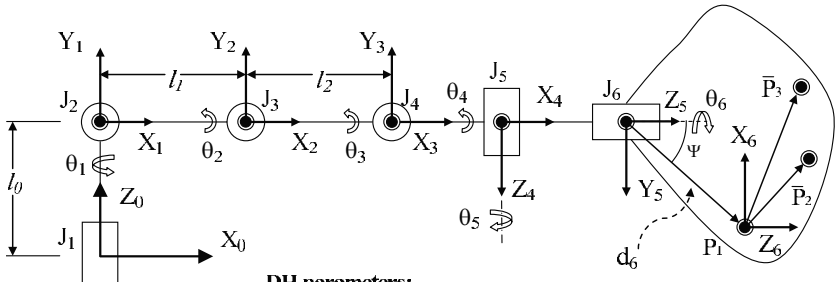

DH parameters:

Link	1	2	3	4	5	6
ai	0	l_1	l_2	0	0	$(d6)\sin(\psi)$
αi	π/2	0	0	π/2	π/2	0
di	l_0	d_2	0	0	0	$(d6)\cos(\psi)$
θi	θ1	θ2	θ3	θ4	θ5 + π/2	θ6 - π/2

Fig. 1 A six-revolute robot. Reference frames 3–5 are centered at the wrist. They are drawn separately for clarity. The wrist center is used as a control point, so $\Psi=0$ and $d_6=0$.

$$\frac{d}{dq_1}\|\bar{P}_i(q_i)-\bar{P}_1(q_1)\|=\frac{d}{dq_1}\|\bar{P}_i(q_i^*)-\bar{P}_1(q_1^*)\|=0$$

$$\Rightarrow(\bar{P}_i(q_i)-\bar{P}_1(q_1))\cdot\left(\frac{d\bar{P}_i}{dq_i}\frac{dq_i}{dq_1}-\frac{d\bar{P}_1}{dq_1}\right)=0$$

$$\Rightarrow \left.\frac{dq_i}{dq_1}\right|_{q_1^*}=\frac{(\bar{P}_i(q_i^*)-\bar{P}_1(q_1^*))\cdot\left.\dfrac{d\bar{P}_1}{dq_1}\right|_{q_1^*}}{(\bar{P}_i(q_i^*)-\bar{P}_1(q_1^*))\cdot\left.\dfrac{d\bar{P}_i}{dq_i}\right|_{q_i^*}} \tag{38}$$

This determines $\mathbf{J}$ at the current configuration.

The column vector $\mathbf{P}'$ contains scalar multiples of the desired tangents at the three control points consistent with the RBC. For nonsingular configurations of the robot, rank$[\mathbf{J}']=6$ and $\mathbf{P}' \in col[\mathbf{J}']$. Therefore, rank$[\mathbf{J}]=6$. The robot is in an ordinary, first-order singular configuration when rank$[\mathbf{J}']=5$ and $\mathbf{P}' \notin col[\mathbf{J}']$. Again, rank$[\mathbf{J}]=6$. Therefore, for nonsingular as well as ordinary, first-order singular configurations, the solution curve in Eq. (36) can be described using one of the motion variables. A similar argument can be constructed for the three-DOF case developed in the previous sections.

Consistent with the development for the three-DOF case, a leading joint variable (θ_1) is used to parameterize the solution curve. Furthermore, the derivatives of the path variables u_i are treated as independent unknowns, although their differentials are related to the derivatives of q_i (e.g., $(u_1/u_2)=(dq_1/dq_2)$). This way, the formulation developed for the three-DOF case can be utilized without alteration, and the following pth-order coordination equation in the general form is obtained by simply concatenating Eq. (13) applied to the three control points

$$\mathbb{J}\bar{n}_p^*=\bar{\Psi}_{p-1} \tag{39}$$

where

$$\mathbb{J}:=\begin{bmatrix}\mathbf{J}_1^* & -\hat{T}_1 & \bar{0} & \bar{0}\\ \mathbf{J}_2^* & \bar{0} & -\hat{T}_2 & \bar{0}\\ \mathbf{J}_3^* & \bar{0} & \bar{0} & -\hat{T}_3\end{bmatrix},\quad \bar{\Psi}_{p-1}:=\begin{bmatrix}\bar{\Psi}_{1(p-1)}\\ \bar{\Psi}_{2(p-1)}\\ \bar{\Psi}_{3(p-1)}\end{bmatrix}$$

$$\bar{n}_p^*:=[n_2^{(p)}\ \ n_3^{(p)}\ \ n_4^{(p)}\ \ n_5^{(p)}\ \ n_6^{(p)}\ \ u_{1p}\ \ u_{2p}\ \ u_{3p}]^T$$

where the quantities u_{ip} and $\bar{\Psi}_{i(p-1)}$ are the pth-derivative of the path variable with respect to the leading joint variable and the RHS of the coordination equation as defined for the three-DOF case applied to point i, respectively, and $\mathbf{J}_i^*$ is a 3×5 matrix obtained by deleting the column of the Jacobian corresponding to the leading joint. Equation (39) is solved by computing the pseudoinverse of the 9×8 matrix $\mathbb{J}$. Equation (39) is used in the example provided in Sec. 4.

Ordinary singularities in any one of the three Jacobians $\mathbf{J}_i$ or the Jacobian $\mathbf{J}'$ will invoke the singularity solution, and the path velocities u_{1i} will vanish. Also, the matrix $\mathbb{J}$ drops rank if $\hat{T}_i$ vanishes. This happens when the corresponding control point lies on the instantaneous screw axis of a pure rotational motion of the EE. If one (or two) tangent(s) vanish, the corresponding path derivatives, $u_{ip}=0$ (and $u_{jp}=0$), $\forall p$. Therefore, the column(s) containing $\hat{T}_i$ (and $\hat{T}_j$) can be deleted from $\mathbb{J}$, and the terms u_{ip} (and u_{jp}) can be deleted from $\bar{n}_p^*$. The resulting linear system of nine equations with seven (or six) unknowns can be solved. However, if all three control points have instantaneous dwells in their trajectories, all tangents $\hat{T}_i=\bar{0}$, $\Rightarrow$rank$[\mathbb{J}]=5$. This condition occurs when the control points lie on the instantaneous screw axis of a pure rotational motion. Choosing noncollinear control points will ensure that all tangents never vanish simultaneously. This condition on the choice of control points resonates with the result in Ref. [32] mentioned earlier in this section.

4 Example

The following example solves the complete trajectory-tracking problem by generating local solutions to the geometric and the temporal tracking subproblems and then using a feedback controller to compensate for tracking errors. To show how the methodology developed in this paper can be used in conjunction with existing feedback paradigms, a conventional resolved-acceleration feedback controller [3] is employed. The output of the controller is interpreted in a natural way to serve as the input to the inverse-kinematic problems in the appropriate form.

A six-DOF manipulator, along with its DH parameters as per Ref. [2], is shown in Fig. 1. The shoulder joint consists of two revolutes (θ_1 and θ_2) with intersecting axes, the elbow joint is a single revolute (θ_3), and the wrist has three revolute joints (θ_4

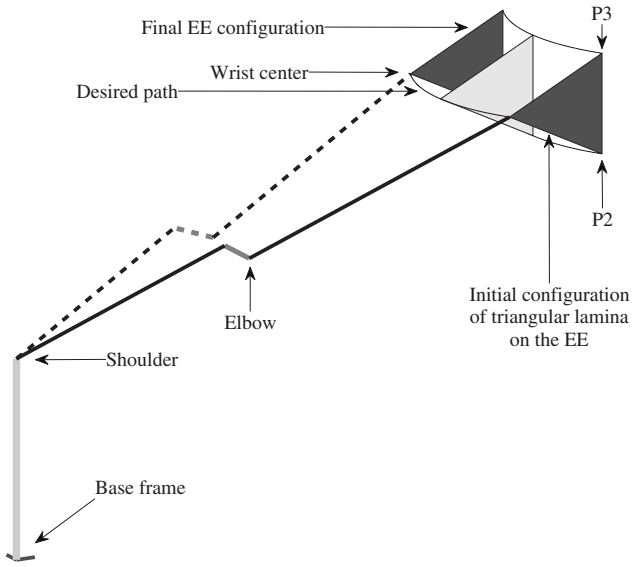

Fig. 2 The three control points on the EE form a triangular lamina. The initial, final, and an intermediate position of the lamina are indicated. The orientation of the EE must be constant during the motion, so all control points follow identical paths.

$-\theta_6$) with axes intersecting at the wrist center. The wrist center, used as a control point, along with two more points on the EE forms a triangular lamina. The robot wrist tracks a circular trajectory parallel to the X_0Y_0 plane while maintaining the orientation of the EE. This is illustrated in Fig. 2. The initial joint angles are $\theta_{i0}=[0\ \ 20\ \ 0\ \ 40\ \ 20\ \ -60]$ deg. The regional structure of the robot is singular in the initial and final configurations, i.e., $\theta_{3\ \text{initial}}=\theta_{3\ \text{final}}=0$. The parameters of the robot are $l_0=1$, $l_1=1.2$, $l_2=1.5$, $d_2=0.25$ in arbitrary length units. The desired trajectories of the control points in appropriate length units are

$$\bar{P}_1(t)=\begin{bmatrix}3.3333\\0.2549\\1.9235\end{bmatrix}+0.94\begin{bmatrix}\cos(q(t))\\\sin(q(t))\\0\end{bmatrix}$$

$$\bar{P}_2(t)=\bar{P}_1(t)+[0.5\quad 0\quad -0.25\,]^T,\quad \text{and}$$

$$\bar{P}_3(t)=\bar{P}_1(t)+[0.5\quad 0\quad 0.25\,]^T$$

where $q(t)=0.0456t^3-0.2394t^2+3.7068$. The EE velocity at the start and the end of motion is zero. The motion is executed in 3.5 s. The shoulder joint θ_2 is the leading joint variable for the entire motion.

The position and velocity gains for the controller are $k_p=250\ \text{s}^{-2}$ and $k_v=70\ \text{s}^{-1}$, respectively, and the feedback frequency is 90 Hz. The joint velocities and accelerations are limited to 15 rad/s and 15 rad/s^2, respectively. As the robot moves, the control points generate trajectories $\bar{r}_i$. At each time instant t^*, position and velocity tracking errors are defined as $\bar{e}_i=\bar{r}_i(t^*)-\bar{P}_i(t^*)$ and $\dot{\bar{e}}_i=\dot{\bar{r}}_i(t^*)-\dot{\bar{P}}_i(t^*)$, respectively, for each control point. The controller corrects for these errors by maintaining the current tangent directions and redefining the desired accelerations as $\ddot{\bar{P}}_i^*:=\ddot{\bar{P}}_i(t^*)-k_v\dot{\bar{e}}_i-k_p\bar{e}_i$. Geometric motion properties of the control points up to the second order are obtained via Eqs. (4)–(6), and the corresponding speed ratios are obtained using Eq. (39). The leading joint motion is obtained via Eqs. (20) and (21) applied to the wrist, following which, the temporal motions of the remaining joints are obtained using equations of the form (23) and (24).

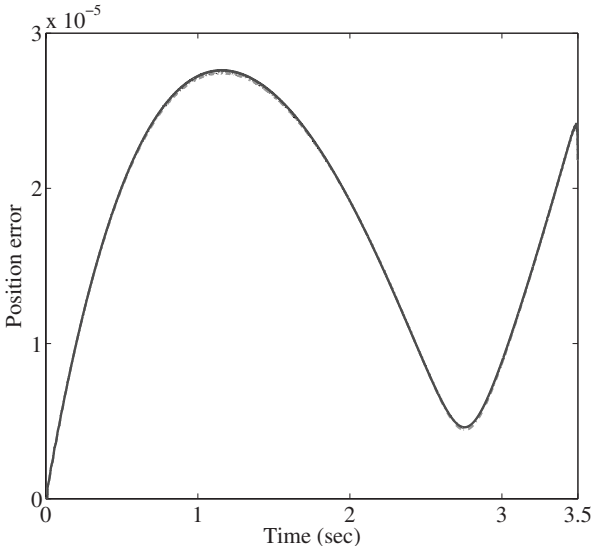

Fig. 3 Position error for the three control points, as shown here, are close to each other. The maximum error is 2.6×10^{-5} units.

The configuration at $t=0$ represents an ordinary singularity because $\text{rank}[\mathbf{J}_1]=2$, $\hat{T}_1\notin col[\mathbf{J}_1]$, and therefore $\text{rank}[\mathbf{J}]=6$. The only change in the strategy mentioned previously is that now Eqs. (32) and (33) are used to obtain the leading joint temporal motion. Since the desired speed at $t=0$ is zero, matching the acceleration and jerk of the desired and generated paths provides exact solutions for the leading joint velocity and acceleration. Note that toward the end of the motion, the robot gets arbitrarily close to the singularity but does not reach the singular configuration, so that the computation strategy does not change once the robot has moved away from the singular configuration at $t=0$.

The performance of the algorithm is illustrated in Figs. 3 and 4. Figure 3 plots the position errors $\bar{e}_i(t)$ for all control points. Note that the error around $t=0$ is low, indicating that both the geometry and the speed of the desired motion is successfully approximated near the singular configuration. The corresponding joint velocities, given in Fig. 4, are well below the established limit. The slope of

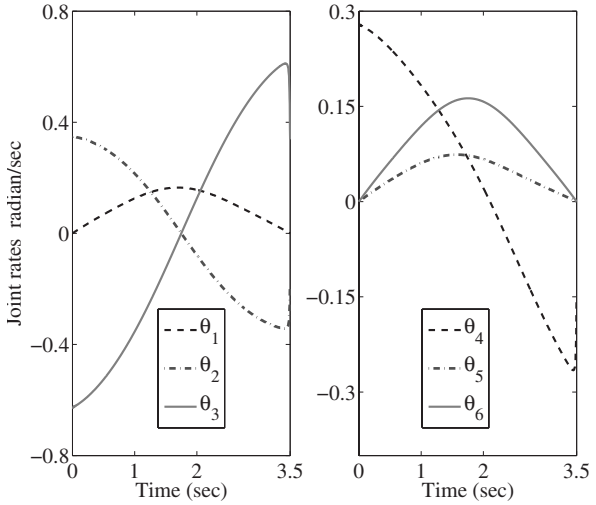

Fig. 4 Joint velocities for the tracking task. The velocities are bounded throughout the task. The slope of the profiles indicates the joint accelerations. The accelerations are high toward the end of the motion for θ_2, θ_3, and θ_4 .

the velocity curves indicate that none of the joint accelerations reach the acceleration limit. The accelerations are highest toward the end of motion when the robot is approaching the singularity, although, the acceleration limit was reached only for joint angle θ_3.

High feedback frequency and feedback gains are used in the above example to illustrate that the robot can approach the singular configuration without the joint motion becoming large. At $t=3.5$, $\theta_3=0.26$ deg, and the position error is 2×10^{-5} units. Simulations with a feedback frequency of 30 Hz and gains $k_p=50\ \text{s}^{-2}$ and $k_v=20\ \text{s}^{-1}$ resulted in a maximum position error of the order of 10^{-3} length units. In conclusion, the robot successfully navigates away from the singularity ($t\approx0$), comes arbitrarily close to the singularity ($t\approx3.5$), and navigates the entire path with small position error (maximum position error$=2.6\times10^{-5}$ length units) and bounded joint motions.

5 Discussion

The implementation of the algorithm developed in this paper requires description of motion in finer detail with its geometric and temporal aspects separated at the problem specification stage and the implementation stage. This requires reworking the task specifications from existing formats, and it increases the computational complexity of the algorithm. Inversion of the Jacobian of the kinematic map rather than the manipulator Jacobian is required, and therefore, it is difficult to provide a comprehensive complexity analysis here. However, the computation of the speed ratios will be roughly the most computationally expensive operation in this algorithm. The advantage of singularity navigation also comes at the cost of increased computation. Recall that third-order coordination is required to obtain the joint velocities and accelerations for singular configurations of the robot. However, the computational effort involved is not forbidding, since the simulation results presented here were developed on a standard desktop computer using MATLAB-RELEASE 2009a. The computation of the joint motions required approximately 0.01 s, indicating that the algorithm can be implemented in real time with the use of dedicated, application-specific software and hardware. Finally, the controllers for the three control points employ identical gains in the presented example. The choice of these gains for various tracking tasks can be viewed as a challenge as well as design flexibility.

The matching of higher-order motion properties opens up the possibility of substantially decreasing the feedback frequency. Then, the system evolves as a combination of continuous dynamics (the evolution of the joint angles) and a sequence of discrete events (feedback-based correction). Constructing control schemes for this hybrid system (see Ref. [33], for example) and studying their stability are interesting problems for future investigation.

6 Conclusions

A methodology was developed to solve the geometric path-tracking problem using three-DOF nonredundant spatial robots to an arbitrary order. The method was extended to the six-DOF rigid-body-guidance problem by writing the kinematic equations of motion developed for the three-DOF case for three noncollinear points in the EE. Path timing was added to the geometric solution, and in particular, a methodology was provided for obtaining the time derivatives of the joint variables for ordinary singularities. Trajectory tracking with this approach, in conjunction with resolved-rate acceleration control, was demonstrated using a spatial 6R robot. Simulation results indicated that the joint velocities and accelerations remain bounded while starting from and approaching a singular configuration. The approach can be computationally demanding; however, the simulation times indicate that it can be effectively employed for physical systems.

Appendix A

It is shown that the pth-order coordination equation is always linear in the pth-order speed ratios. The forward kinematic map can be viewed as a composite function with a vector argument: $\bar{r}(\lambda)=\bar{r}(\mu(\lambda),\nu(\lambda),\lambda(\lambda))$, where $\mu(\lambda)$ and $\nu(\lambda)$ are the Taylor series given by Eq. (1). When all the appropriate derivatives are defined, the generalized Faa di Bruno formula is used to obtain the pth-derivative of a component r_m $(m=1,2,3)$ of $\bar{r}(\lambda)$ as [34]

$$\frac{d^p r_m}{d\lambda^p}=\sum_0\sum_1\sum_2\cdots\sum_p\left(\frac{p!}{\prod_{i=1}^{p}(i!)^{g_i}\prod_{i=1}^{p}\prod_{i=1}^{3}q_{ip}!}\times\frac{\partial^f r_m}{\partial\lambda^{p_1}\,\partial\mu^{p_2}\,\partial\nu^{p_3}}\right)\times\prod_{i=1}^{p}(\lambda^{(i)})^{q_{i1}}(\mu^{(i)})^{q_{i2}}(\nu^{(i)})^{q_{i3}} \tag{A1}$$

where the respective sums are over all non-negative integer solutions of the Diophantine equations as follows:

$$\begin{aligned}\sum_0 &\rightarrow g_1+2g_2+3g_3+\cdots+pg_p=p\\ \sum_1 &\rightarrow q_{11}+q_{12}+q_{13}=g_1\\ \sum_2 &\rightarrow q_{21}+q_{22}+q_{23}=g_2\\ &\vdots\\ \sum_p &\rightarrow q_{p1}+q_{p2}+q_{p3}=g_p\end{aligned} \tag{A2}$$

and p_1, p_2, and p_3, the orders of partial derivatives with respect to λ, μ, and ν, respectively, and f, the order of the partial derivative, are

$$p_e=q_{1e}+q_{2e}+\cdots+q_{pe},\quad e=1,2,3$$

$$f=p_1+p_2+p_3=\sum_{i=1}^{p}g_i$$

and $\mu^{(i)}:=(d^i\mu/d\lambda^i)$. Thus, only the last term in Eq. (A1) consists of the speed ratios. The condition $i=p$ gives the highest-order speed ratio. Next, note that the sum Σ_0 in Eq. (A2) implies that g_p can have no solution other than $g_p=0$ or 1. This, along with the sum Σ_p in Eq. (A2) implies that only one of the powers q_{p1}, q_{p2}, and q_{p3} can equal 1, and the other two must be zero. Therefore, for $i=p$, only one of the speed ratios in the last term of Eq. (A1) will remain and the others will equal 1. Therefore, the pth-derivative of r_m will be linear in the pth-order speed ratios.

Appendix B: Speed Ratios From Time-Based Joint Motions

When the pth-order time-based solution for the joint motions exists, an alternative way to obtain the speed ratios is by differentiating the Taylor series in Eq. (1) with respect to time t. The differentiation can be carried out using Faa di Bruno's formula [35] for the pth-order differentiation of composite functions. For example, the pth-order differentiation of the composite function $\mu(\lambda(t))$ with respect to t is given by

$$\frac{d^p\mu}{dt^p} = \sum \frac{p!}{g_1! \dots g_p!} \times \frac{d^g\mu}{d\lambda^g} \times \left(\frac{d\lambda/dt}{1!}\right)^{g_1} \dots \left(\frac{d^p\lambda/dt^p}{p!}\right)^{g_p} \tag{B1}$$

where the sum is over all different solutions in nonnegative integers $g_1, \dots, g_p$ of $g_1+2g_2+\cdots+pg_p=p$, and $g := g_1+\cdots+g_p$. Note that $g \le p$. Furthermore, in the zero position, the term $(d^g\mu/d\lambda^g)$ is the gth-order speed ratio. Also, for $g=p$

$$g_1 + g_2 + \cdots + g_p = p$$

$$g_1 + 2g_2 + \cdots + pg_p = p$$

$$\Rightarrow g_2 + 2g_3 + \cdots + (p-1)g_p = 0$$

$$\Rightarrow g_i = 0, \quad \text{for} \quad i = 2,3, \dots p, \quad \text{and} \quad g_1 = p$$

Therefore, for $g=p$, the sum in Eq. (B1) reduces to $n^{(p)}(\dot{\lambda})^p$ in the zero position. Equation (B1) can now be written as

$$\left.\frac{d^p\mu}{dt^p}\right|_0 = \sum \frac{p!}{g_1! \dots g_p!} \times n^{(g)} \times \left(\frac{d\lambda/dt}{1!}\right)^{g_1} \dots \left(\frac{d^p\lambda/dt^p}{p!}\right)^{g_p} + n^{(p)} \times (\dot{\lambda})^p$$

$$\Rightarrow n^{(p)} = \frac{1}{(\dot{\lambda})^p} \times \left\{ \left.\frac{d^p\mu}{dt^p}\right|_0 - \sum \frac{p!}{g_1! \dots g_p!} \times n^{(g)} \times \left(\frac{d\lambda/dt}{1!}\right)^{g_1} \dots \left(\frac{d^p\lambda/dt^p}{p!}\right)^{g_p} \right\} \tag{B2}$$

where $g \le p-1$. Equation (B2) obtains the pth-order ratio as a function of the previous $p-1$ ratios and the time derivatives of the joint variables up to the pth order.

Appendix C: Nonordinary Singularity

A bifurcation or nonordinary singularity occurs when $\mathbf{J}$ is rank deficient and $\hat{T} \in col[\mathbf{J}]$. Reference [28] provides means for offline planning and analysis of bifurcations. This Appendix provides the rudiments of an algorithm for online trajectory tracking through nonordinary singularities. Detailed study of this issue is a subject for future work. A nonordinary singularity can be distinguished from an ordinary singularity by constructing the augmented matrix $\mathbf{J}^\dagger := [\mathbf{J} \ \hat{T}]$. Then, if $\text{rank}[\mathbf{J}^\dagger]=3$, the singularity is ordinary. If $\text{rank}[\mathbf{J}^\dagger]=2$, the singularity is nonordinary. For nonordinary singularities, it is possible to track the desired tangent with first-order joint coordination. Therefore, the governing coordination equation should match the direction of $\bar{r}_{\lambda 0}$ with $\hat{T}$. However, Eq. (14) is not useful since it is not possible to construct $\mathbf{J}^*$ that is full rank. The first-order speed ratios are obtained from Eq. (12) with $p=1$ as follows:

$$\mathbf{J}\bar{n}_1 = u_1\hat{T}$$

$$\therefore \hat{T} \times (\mathbf{J}\bar{n}_1) = u_1(\hat{T} \times \hat{T}) = \bar{0}, \quad \Rightarrow [\mathbf{TJ}]\bar{n}_1 = \bar{0} \tag{C1}$$

where $\mathbf{T}$ is the skew-symmetrization of $\hat{T}$. It can be shown that for a nonordinary singularity, $\text{rank}[\mathbf{TJ}]=1$. Therefore, Eq. (C1) yields one linear equation in the two speed ratios: $n+a_1k+b_1=0$, where a_1 and b_1 are scalar coefficients determined by $\mathbf{T}$ and $\mathbf{J}$. The coefficient u_1 is obtained as

$$u_1 = \mathbf{J}\left\{ n\begin{bmatrix} 1 \\ -\frac{1}{a_1} \\ 0 \end{bmatrix} + \begin{bmatrix} 0 \\ -\frac{b_1}{a_1} \\ 1 \end{bmatrix} \right\} \cdot \hat{T} \tag{C2}$$

A unique solution for the first-order speed ratios and u_1 can be obtained by considering the second-order coordination equation, which, after cross multiplying Eq. (12) ($p=2$) with the tangent vector is expressed as

$$\hat{T} \times (\mathbf{J}\bar{n}_2) - \kappa u_1^2 \hat{B} = -\hat{T} \times \bar{\Phi}_1 \tag{C3}$$

Clearly, all three vectors in Eq. (C3) belong to the $\hat{N}-\hat{B}$ plane. The RHS is a known vector. In the left-hand side (LHS), the first term is a vector perpendicular to the two-dimensional column-space of $\mathbf{J}$. Therefore, it has a fixed direction, and its coefficient is a function of the two second-order speed ratios. The second term in the LHS is also a vector with fixed direction and a variable magnitude that depends on the variable u_1. Equation (C3) is therefore a planar vector loop equation that can be solved for the coefficients of the vectors in the LHS. The coefficient of the first term defines a single infinity of solutions for the second-order speed ratios, and the coefficient of the second term yields a value for u_1. Assuming that $u_1^2 > 0$ (a negative value is not expected; however, this is a subject for future work), u_1 is the positive square root since, by definition, u_1 is the rate of change of the arc length, and a positive value of u_1 indicates that the EE is progressing in the desired direction. This value of u_1 provides a unique solution for n via Eq. (C2), and then, k is obtained from Eq. (C1). An expression for the coefficient u_2 can be obtained from Eq. (12) (with $p=2$) by taking a dot product with $\hat{T}$. As before, the third-order coordination equation will resolve the redundancy in the second-order solution and simultaneously provide a single infinity of solutions for the third-order speed ratios and the coefficient u_3.

In the vicinity of a nonordinary singularity, all possible matrices $\mathbf{J}^*$ will be ill conditioned. The solution methodology described here can be implemented in a suitable neighborhood of the bifurcation.

References

[1] Chiaverini, S., Oriolo, G., and Walker, I. A. D., 2008, *Springer Handbook of Robotics*, B. Siciliano and O. Khatib, eds., Springer Verlag, Western Europe, Chap. 11, pp. 245–268.

[2] Spong, W. M., Hutchinson, S., and Vidyasagar, M., 2006, *Robot Modeling and Control*, Wiley, New York.

[3] Caccavale, F., Natale, C., Siciliano, B., and Villani, L., 1998, "Resolved-Acceleration Control of Robot Manipulators: A Critical Review With Experiments," Robotica, **16**, pp. 565–573.

[4] Kieffer, J., and Litvin, F. L., 1991, "Local Parametric Representation of Displacement Functions for Linkages and Manipulators," Mech. Mach. Theory, **26**(1), pp. 41–53.

[5] Lloyd, J., 1995, "Robot Trajectory Generation for Paths With Kinematic Singularities," Ph.D. thesis, McGill University, Montreal, Canada.

[6] Chiaverini, S., Sciavicco, L., and Siciliano, B., 1991, "Control of Robotic Systems Through Singularities," *Advanced Robot Control, Vol. 162 of Lecture Notes in Control and Information Sciences*, Springer, Berlin/Heidelberg, pp. 285–295.

[7] Wolovich, W. A., and Elliot, H., 1984, "A Computational Technique for Inverse Kinematics," Proceedings of the 23rd IEEE Conference on Decision and Control, pp. 1359–1363.

[8] Wampler, C. W., II, and Leifer, L. J., 1988, "Application of Damped Least-Squares Methods to Resolve-Rate and Resolved-Acceleration Control of Manipulators," ASME J. Dyn. Syst., Meas., Control, **110**(1), pp. 31–38.

[9] Nenchev, D. N., Tsumaki, Y., and Uchiyania, M., 1996, "Adjoint Jacobian Closed-Loop Kinematic Control of Robots," Proceedings of the IEEE International Conference on Robotics and Automation, pp. 1235–1240.

[10] Kieffer, J., 1992, "Manipulator Inverse Kinematics for Untimed End-Effector Trajectories With Ordinary Singularities," Int. J. Robot. Res., **11**(3), pp. 225–237.

[11] Lloyd, J. E., 1998, "Desingularization of Nonredun-Dant Serial Manipulator Trajectories Using Puiseux Series," IEEE Trans. Rob. Autom., **14**(4), pp. 590–600.

[12] Nenchev, D. N., 1995, "Tracking Manipulator Trajectories With Ordinary Singularities: A Null Space-Based Approach," Int. J. Robot. Res., **14**(4), pp. 399–404.

[13] Tumeh, Z. S., and Alford, C. O., 1988, "Solving for Manipulator Joint Rates in Singular Positions," Proceedings of the IEEE International Conference on Robotics and Automation, pp. 987–992.
[14] Ghosal, A., and Ravani, B., 2001, "A Differential-Geometric Analysis of Singularities of Point Trajectories of Serial and Parallel Manipulators," ASME J. Mech. Des., **123**(1), pp. 80–89.
[15] Lloyd, J. E., and Hayward, V., 2001, "Singularity-Robust Trajectory Generation," Int. J. Robot. Res., **20**(1), pp. 38–56.
[16] Atkeson, C. G., and Hollerbach, J. M., 1985, "Kinematic Features of Unrestrained Vertical Arm Movements," J. Neurosci., **5**(9), pp. 2318–2330.
[17] Ambike, S., and Schmiedeler, J. P., 2006, *Advances in Robot Kinematics*, J. Lenarčič and B. Roth, eds., Springer, Dodrecht, pp. 177–184.
[18] Dounskaia, N., 2005, "The Internal Model and the Leading Joint Hypothesis: Implications for Control of Multi-Joint Movements," Exp. Brain Res., **166**(1), pp. 1–16.
[19] Bottema, O., and Roth, B., 1979, *Theoretical Kinematics*, North Holland, Amsterdam.
[20] Lorenc, S. J., Stanišić, M. M., and Hall, A. S. J., 1995, "Application of Instantaneous Invariants to the Path Tracking Control Problem of Planar Two Degree-of-Freedom Systems: A Singularity-Free Mapping of Trajectory Geometry," Mech. Mach. Theory, **30**(6), pp. 883–896.
[21] Roth, B., and Yang, A. T., 1977, "Application of Instantaneous Invariants to the Analysis and Synthesis of Mechanisms," ASME J. Eng. Ind., **99**(1), pp. 97–103.
[22] Stanišić, M. M., Lodi, K., and Pennock, G. R., 1992, "Application of Curvature Theory to the Trajectory Generation Problem of Robot Manipulators," ASME J. Mech. Des., **114**(4), pp. 677–680.
[23] Lorenc, S. J., and Stanišić, M. M., 1994, "Third-Order Control of a Planar System Tracking Constant Curvature Paths," *Advances in Robot Kinematics and Computational Geometry*, J. Lenarcic and B. Ravani, eds., Kluwer Academic, Dodrecht, pp. 229–238.
[24] Lorenc, S. J., and Stanišić, M. M., 1994, "Second Order Geometry-Based Path Tracking of Industrial Arm Sub-Assemblies," 23rd ASME Biennial Mechanisms Conferences, Vol. 72, pp. 301–306.
[25] Golubitsky, M., and Guillemin, V., 1973, *Stable Mappings and Their Singularities*, Springer Verlag, New York.
[26] Kreyszig, E., *Differential Geometry*, 1964, University of Toronto Press, Toronto.
[27] Ambike, S., Schmiedeler, J. P., and Stanišić, M. M., 2010, "Geometric, Spatial Path Tracking and Rigid-Body Guidance Using Non-Redundant Manipulators via Speed-Ratio Control," ASME Paper No. DETC2010-28061.
[28] Kieffer, J., 1994, "Differential Analysis of Bifurcations and Isolated Singularities of Robots and Mechanisms," IEEE Trans. Rob. Autom., **10**(1), pp. 1–10.
[29] Klein, C. A., and Blaho, B. E., 1987, "Dexterity Measures for the Design and Control of Kinematically Redundant Manipulators," Int. J. Robot. Res., **6**(2), pp. 72–83.
[30] Yoshikawa, T., 1985, "Manipulability of Robotic Mechanisms," Int. J. Robot. Res., **4**(2), pp. 3–9.
[31] Angeles, J., Rojas, A., and López-Cajún, C. S., 1988, "Trajectory Planning in Robotics Continuous-Path Applications," IEEE Trans. Rob. Autom., **4**(4), pp. 380–385.
[32] Gosselin, C. M., 1990, "Dexterity Indices for Planar and Spatial Robotic Manipulators," Proceedings of the IEEE International Conference on Robotics and Automation, pp. 650–655.
[33] Kolmanovsky, I., Reyhanoglu, M., and McClamroch, N. H., 1994, "Discontinuous Feedback Stabilization of Nonholonomic Systems is Extended Power Form," Proceedings of the 33rd IEEE Conference on Decision and Control, pp. 3469–3475.
[34] Mishkov, R. L., 2000, "Generalization of the Formula of Faa di Bruno for a Composite Function With a Vector Argument," Int. J. Math. Math. Sci., **24**(7), pp. 481–491.
[35] Johnson, W. P., 2002, "The Curious History of Faa di Bruno's Formula," Am. Math. Monthly, **109**, pp. 217–234.